Wave-pinned filaments of scroll waves

Tamás Bánsági, Jr., Kevin J. Meyer, and Oliver Steinbock[a)]
Department of Chemistry and Biochemistry, Florida State University, Tallahassee, Florida 32306-4390, USA

(Received 5 November 2007; accepted 26 December 2007; published online 6 March 2008)

Scroll waves are three-dimensional excitation patterns that rotate around one-dimensional space curves. Typically these filaments are closed loops or end at the system boundary. However, in excitable media with anomalous dispersion, filaments can be pinned to the wake of traveling wave pulses. This pinning is studied in experiments with the 1,4-cyclohexanedione Belousov–Zhabotinsky reaction and a three-variable reaction-diffusion model. We show that wave-pinned filaments are related to the coexistence of rotating and translating wave defects in two dimensions. Filament pinning causes a continuous expansion of the total filament length. It can be ended by annihilating the pinning pulse in a frontal wave collision. Following such an annihilation, the filament connects itself to the system boundary. Its postannihilation shape that is initially the exposed rim of the scroll wave unwinds continuously over numerous rotation periods. © *2008 American Institute of Physics*. [DOI: 10.1063/1.2835602]

I. INTRODUCTION

Rotating spiral waves are a common phenomenon in a broad spectrum of experimental systems. Examples from physics and chemistry include Rayleigh–Bénard convection,[1] dielectric barrier discharge in gases,[2] corroding metal surfaces under thin electrolyte layers,[3] catalytic surface reactions such as CO oxidation on Pt,[4] and the homogeneously catalyzed Belousov–Zhabotinsky (BZ) reaction.[5] In particular, spiral waves in the latter two examples share profound similarities with rotors in certain biological systems. Classic examples are spiral waves in aggregating populations of the cellular slime mold *Dictyostelium discoideum*,[6] the interior of fertilized egg cells,[7] the retina of chicken,[8] cardiac tissue, and the human heart where rotating waves of action potential are believed to cause ventricular arrhythmia and fibrillation.[9]

Most of the latter systems behave as excitable media. In the simplest case, they have a single, stable steady state. However, perturbations exceeding a characteristic threshold cause the system to perform a long excursion through phase space prior to returning to the rest state. During the latter phase of this cycle, the excitation threshold is raised and the system is refractory. In spatially extended media with appropriate short-range coupling such as diffusion, the excitation cycle spreads through space at a constant speed.[10] This propagation is driven by steep gradients at the wave front, which induce fluxes and perturb areas ahead of the front. The resulting wave pulse spatially unfolds the excitation cycle and causes a refractory zone in the wave back. Consequently, colliding excitation waves show no interference phenomena but annihilate in response to frontal wave-to-wave and wave-to-obstacle collisions.[11]

The refractory zone and its specific relaxation dynamics are of critical importance to the structure and dynamics of wave trains. For example, they create a wavelength λ_{min} below which no wave trains can exist. Moreover, in many experimental systems, the wave speed increases with increasing wavelengths and saturates at a finite, maximal value that equals the velocity of a solitary pulse propagating into a fully recovered medium.[12,13] This simple dependence of wave velocity c on wavelength λ is often referred to as normal dispersion. However, numerous theoretical as well as experimental studies have documented interesting "anomalies" of $c(\lambda)$, such as damped oscillations, band gaps, finite bandwidths, and bistability.[14–17]

One of these so-called anomalous dispersion relations gives rise to a phenomenon known as "wave merging."[18,19] In this case, the dispersion relation has a single maximum and the speed $c(\lambda_{min})$ is larger than the velocity of the solitary pulse, which implies that the frontier pulse is the slowest pulse in every finite wave train.[19,20] Consequently, all trailing pulses approach the wake of the frontier pulse where they disappear. Nonetheless, wave trains and patterns can obviously expand in size and overall number of pulses.

We investigate the dynamics of rotating spiral waves in excitable reaction-diffusion media with the latter type of anomalous dispersion.[21] In two-dimensional systems, these patterns are organized by spiral tips that orbit along trajectories such as circles, epicycles, and hypocycles. If the diameter of the tip orbit is small compared to the wavelength of the spiral wave, the trajectory can be represented by its central point. This point is a phase singularity as the pattern's local oscillation phase varies continuously from $-\pi$ to π around closed paths surrounding it.

In three-dimensional systems similar relations hold but here spirals rotate around one-dimensional space curves rather than points. These curves are commonly referred to as "filaments." In general, they are not stationary but evolve according to factors such as local curvature and twist, with the latter denoting gradients in rotation phase.[22–26] For many years, it was believed that filaments must either end at the system boundary or close in on themselves. If closed, they

[a)]Electronic mail: steinbck@chem.fsu.edu.

can form rings, knots, or chain links.[27–29] Recent experiments by our group, however, showed that filaments can also terminate in the wake of a traveling wave pulse if the system obeys dispersion relations giving rise to "wave merging."[30] In this article, we present additional results regarding this unexpected phenomenon and, in particular, reproduce filament pinning by numerical simulations of a three-species reaction-diffusion model.

II. EXPERIMENTAL

We use a modified version of the BZ reaction as our experimental model system. In this reaction, the classic organic substrate and the catalyst are replaced by 1,4-cyclohexanedione (CHD) and $[Fe(batho(SO_3)_2)_3]^{4-}$, respectively. The first substitution excludes undesired bubble formation, while the latter one yields a conveniently large difference between the molar absorption coefficients of the reduced and the oxidized state.[31] More importantly, however, the former substitution gives rise to various types of anomalous dispersion relations, which have been described and analyzed in earlier studies.[19,20] Reaction mixtures are prepared from stock solutions of $NaBrO_3$ (Fluka), CHD (Aldrich), sulfuric acid (Riedel-de Haën, 5 M), catalyst, nanopure water, and polyacrylamide solution. The latter compound increases the viscosity of the BZ solution from about 1 to 150 mPa s suppressing convective fluid motion. The preparation of the catalyst and the polyacrylamide solution is detailed in (Ref. 30).

For pseudo-two-dimensional experiments, the initial concentrations are $[NaBrO_3]=0.20$ mol/l, $[CHD]=0.20$ mol/l, $[H_2SO_4]=0.60$ mol/l, and $[[Fe(batho(SO_3)_2)_3]^{4-}]=0.50$ mmol/l. The latter experiments are carried out in thin layers of the reaction solution confined between two circular plexiglass plates. The height of the solution layer is 0.3 mm. All measurements are carried out at a temperature of 21 ± 1 °C.

For three-dimensional systems, the initial concentrations are $[NaBrO_3]=0.18$ mol/l, $[CHD]=0.19$ mol/l, $[H_2SO_4]=0.60$ mol/l, and $[[Fe(batho(SO_3)_2)_3]^{4-}]=0.475$ mmol/l. After preparing 18 ml of reactant mixture we transfer it to a cylindrical glass cuvette (inner diameter of 3.7 cm). A rod-shaped, magnetic stir bar is fitted to the bottom of this container to remove undesired wave patterns by remixing, which effectively resets the system to a favorable spatially homogeneous state. Two silver wires are utilized to initiate oxidation waves. One wire is attached to a microstage and can be lowered to touch the uncovered BZ solution, while the second one is attached to the top of the magnetic stir bar about 1 mm away from the stir bar's center. Accordingly, the rotation of the stir bar by a few degrees will move the silver wire by a small distance. This feature is essential for initiating the asymmetric spiral patterns to be studied here.

We use optical tomography[32–34] to obtain spatially resolved information on the local absorption within the three-dimensional reaction medium. This technique requires that the reaction cuvette is rotated steadily around its symmetry, or z, axis (typical rotation rate: 12.3 rpm), while transmission images are being acquired at a rate of 12.5 frames/s.

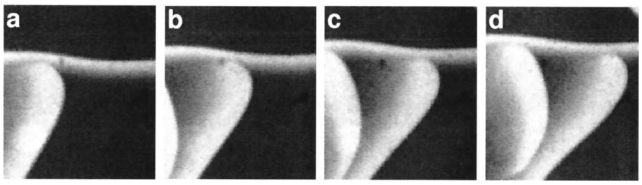

FIG. 1. Sequence of absorption images showing the motion of a nonrotating wave defect in a pseudo-two-dimensional reaction-diffusion system. The defect is pinned to the back of an upward moving, nearly planar wave. Initial reactant concentrations are listed in Sec. II. Time between frames: 10 s. Field of view: 4.3×5.0 mm^2.

To reconstruct the three-dimensional wave pattern, the image data are broken into individual slices, or sinograms, along the vertical rotation axis of the sample. On each sinogram, backprojection[32] is performed to obtain the corresponding concentration field in real space coordinates perpendicular to the z axis. To reduce high wave number artifacts, the sinogram data are processed in the wave number domain using the Ram-Lak filter multiplied by a Hann window.

III. EXPERIMENTAL RESULTS

Pseudo-two-dimensional CHD-BZ media with anomalous dispersion show large-scale target patterns and rotating spiral waves that seem to be qualitatively indistinguishable from those in excitable systems with normal dispersion. However, striking differences exist along the borders of wave patterns expanding into wave-free surroundings. For the specific reagent concentrations studied here, we observe wave merging which means that all trailing pulses eventually disappear in the wake of the outermost frontier pulse. As mentioned in the Introduction, this annihilation zone moves away from the pattern's pacemaker as it is tied to the back of the outermost pulse and eventually vanishes at the system boundary. Prior to this disappearance, remarkable and interesting dynamics can be observed that sometimes also affect later stages by nucleating specific patterns.

A striking example for these phenomena is illustrated in Fig. 1 which shows the propagation of a nonrotating wave defect in a pseudo-two-dimensional CHD-BZ system. The sequence consists of four still frames. The white bands correspond to the excitation waves. Within these brighter regions, the reaction's redox catalyst is predominantly oxidized, while the darker background indicates a chemically more reduced state which is close to the system's stable rest state. In the upper halves of the images, a nearly planar wave pulse propagates in upward direction at a speed of $c_0=20$ μm/s. Below this planar front, two other wave pulses propagate rightward. The latter waves end in the wake of the planar pulse. Closer inspection of the data in Fig. 1 reveals a narrow, dark gap at the T-shaped junctions between the upper and lower waves.

The lower portion of the leading, rightward traveling wave has a nearly linear shape. This segment is oriented at an angle of about 50° with respect to the planar front. This approximate value is reached asymptotically as it is apparent

from the deviations in the early frames in Fig. 1. Furthermore, the wave's leading "head" is clearly convex with its rightmost point being 0.8 mm below the planar front. This head propagates with a velocity of $c_x = 77\ \mu\mathrm{m/s}$ in horizontal direction and, hence, follows a linear trajectory tilted at an angle of $\arctan(c_0/c_x) = 15°$ away from the horizontal. The third pulse trails in the wake of both the planar and the leading rightward moving wave [Figs. 1(b)–1(d)]. In Fig. 1(d) it has not yet reached a stationary shape.

The characteristic geometry of the rightward moving pulses is caused by two main factors: The system's anomalous dispersion and the conventional velocity-curvature dependence of excitation waves. The latter is described by the eikonal equation $N = c_0 - DK$,[35] where N is the normal front velocity, c_0 is the speed of a planar front, and K denotes the fronts local curvature ($K > 0$ for convex fronts). The parameter D is approximately the diffusion coefficient D_u of the system's autocatalytic species (here $HBrO_2$). Accordingly, the convex profile of the head leads to a velocity reduction that partially compensates the higher velocity generated by the head's proximity to the planar, upward moving wave. We note that a similar situation has been studied for the photosensitive BZ reaction where a solitary wave was deformed by a stripe of increased c_0.[36]

Although the analysis of the specific front shape is interesting, it is not further pursued here. In this article, we focus on the pinning of excitation pulses to anchoring planar waves. This pinning creates wave ends that carry out translational rather than rotational motion, which is remarkable because spiral waves can readily form in the very same system. The specific fate of a wave end or wave break appears to be determined by its distance to other wave structures: If the defect is sufficiently far away from other waves, it will curl up to become a rotating spiral; if, however, the defect is initially within the wake of another wave, it is pinned and translates along the back side of its anchoring wave. Notice that this motion can be stopped by collisions with another defect moving in opposite direction. Moreover, wave pinning can also occur in the wake of an expanding, circular anchor wave, which should create defect motion along logarithmic spiral trajectories. We suggest that the critical distance between defect and potential anchor strongly depends on the system's dispersion relation and also on the angle between the waves.

Wave-pinned defects also exist in three-dimensional excitable media. Figure 2 shows a pair of still frames illustrating two different, but nearly simultaneous views through a 3.7 cm thick CHD-BZ system. The viewing angles in frames (a) and (b) differ by 90° with the latter showing a clockwise rotating spiral that ends in the wake of a cusp-shape wave. More importantly, we find that the filament of this three-dimensional spiral wave also terminates at the same wave pattern. However, the positions of the filament's terminal points and the overall shape of scroll wave are not easily discerned from the images in Fig. 2.

We, therefore, compute tomographic reconstructions based on the procedures described in the Experimental section. Two typical examples are shown in Fig. 3 where frames (a) and (b) are obtained from the same wave pattern at two

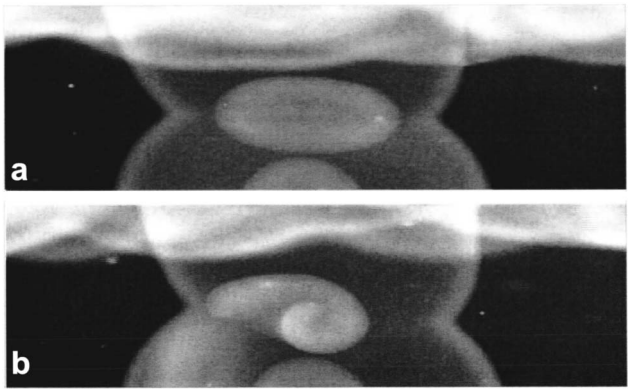

FIG. 2. Two absorption images of an unusual, three-dimensional wave pattern as viewed from two perpendicular directions. The time elapsed between the snapshots is negligible. Initial reactant concentrations are listed in Sec. II. Field of view: $25.9 \times 7.6\ \mathrm{mm}^2$.

different times. In both frames, the entire structure is cut and only the posterior halves are shown. The omitted anterior half is essentially the mirror image of the depicted pattern. The reconstructions reveal that the scroll wave is confined to an hourglass-shaped wave envelope. Furthermore, the outer parts of the scroll wave are connected to the back of this expanding envelope where they undergo dynamics similar to the two-dimensional case shown in Fig. 1. The filament, or rotation backbone, follows the rim of the spiral and also ends in the wake of the envelope wave. Its shape appears to be nearly linear in (a) but bends and wiggles slightly in the course of spiral rotation. Moreover, the filament increases in length as its anchoring wave expands outwards. Additional details of these features have been reported in Ref. 30.

IV. MODEL

Earlier studies show that many of the wave phenomena in the CHD-BZ reaction are captured qualitatively by a simple three-variable reaction-diffusion model.[37,38] These

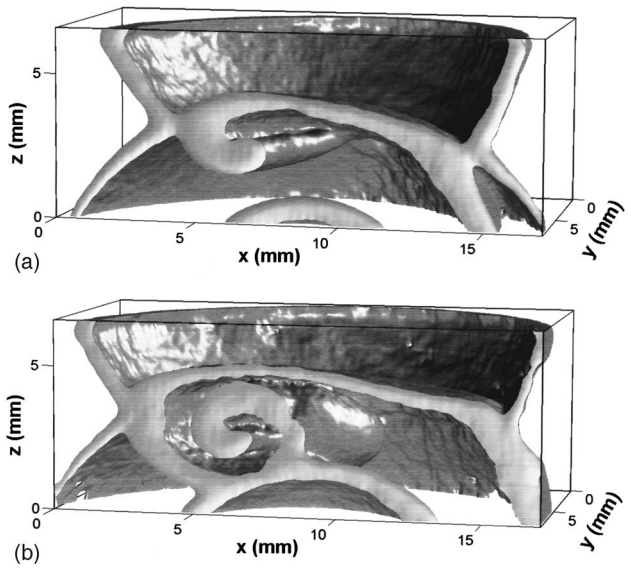

FIG. 3. Tomographic reconstruction of a wave-pinned scroll wave (different from the one shown in Fig. 2). Initial reactant concentrations can be found in Sec. II. Time elapsed between frames: 45 s.

phenomena include wave merging, in general, and more specific features such as the nucleation of spiral pairs in three-wave collisions. The model involves one activator species (u) and two inhibitors (v and w), all of which are functions of the dimensionless time t and the space coordinates x, y, and z,

$$\frac{\partial u}{\partial t} = \nabla^2 u + \frac{1}{\epsilon}\left\{u(1-u)\left(u - \frac{v+w}{a}\right)\right\}, \tag{1}$$

$$\frac{\partial v}{\partial t} = u - v, \tag{2}$$

$$\frac{\partial w}{\partial t} = \beta(\delta - w) - \gamma u w. \tag{3}$$

The parameters ϵ, a, β, γ, and δ are dimensionless constants. For $\delta=0$, Eqs. (1)–(3) are a specific case of the Barkley model.[39] Moreover, Eqs. (1)–(3) are similar but not identical to the Krug model of the photosensitive BZ reaction,[40] which itself is based on the classic Oregonator model.[41] These similarities suggest a qualitative interpretation of u, v, and w as the concentrations of the chemical species $HBrO_2$, oxidized catalyst and Br^-, respectively.

The numerical simulations discussed in the following are carried out for a fixed set of parameter values that defines an excitable system with merging wave pulses and stable spiral waves. The specific model parameters are $\epsilon=0.01$, $a=0.8$, $\beta=0.2$, $\delta=0.51$, and $\gamma=10.0$. The model equations are solved numerically using Euler integration at a grid spacing of 0.2 and a time step of 0.005. Most two- and three-dimensional simulations are carried out on a lattice of 200×200 and $200\times200\times200$ grid points, respectively, constrained by no-flux boundaries.

V. NUMERICAL RESULTS

For spatially one-dimensional systems, the profiles $u(x)$, $v(x)$, $w(x)$ of a typical, traveling pulse have been published in Ref. 37. They show a propagating region of high u values in which the inhibitor w decreases while the inhibitor v increases. In its wake, these changes reverse and set up cross-gradient inhibitor profiles that give rise to the aforementioned anomalies in the dispersion relation of wave trains.

In two-dimensional systems, these features can reproduce the experimentally observed coexistence of translational and rotational wave defects (cf. Fig. 1). Figure 4(a) shows a sequence of three snapshots illustrating the pinning of a fast, rightward moving pulse in the wake of slow planar wave. For this simulation, the latter front was initiated by increasing the value of u along the entire, lower boundary. Once the propagating wave had traveled into the system, the second pulse was triggered along the left boundary up to the position of the planar anchor. The resulting, rightward moving wave rapidly deforms and develops a linear tail and convex head. Its overall shape and the linear trajectory of its upper end are in good agreement with the experimental data shown in Fig. 1.

Figure 4(b) shows the results of a simulation that differs from the one in Fig. 4(a) only by the presence of a second planar wave. This additional wave was initiated along the upper system boundary and propagates downwards. The two planar fronts collide and annihilate, which unpins the rightward moving pulse as shown in the second frame of the sequence. Subsequently, the unpinned wave end stops its translational motion and becomes a rotating, but otherwise stationary, spiral tip. This mechanism of spiral wave nucleation can obviously also occur if the anchoring and annihilating wave pulses are nonplanar.

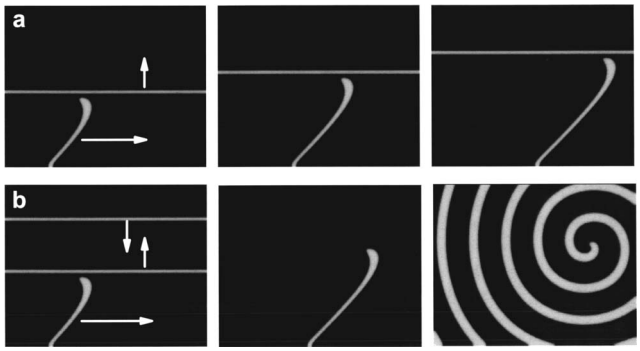

FIG. 4. Results obtained by numerical simulation of Eqs. (1)–(3) for a two-dimensional system. (a) Image sequence of a wave front pinned to the wake of a planar pulse. (b) Spiral formation in response to the annihilation of the pinning wave. Dimensionless time elapsed between the frames is 5.0 in (a) and 7.5 and 48.7 in (b). The area shown in the individual frames measures 50×40.

The two contour plots in Fig. 5 show additional details regarding the similarities of and differences between translational (a) and rotational wave defects (b). Each plot graph curves of constant u (solid line, $u=0.1$) and constant v (dotted and dashed lines, $v=0.1$ and 0.3, respectively). For both types of patterns, the wave ends show a characteristic crossing of lines of constants u and v. This crossing is not observed in other parts of the pattern. Furthermore, the intersection points of the high and low v contours with the u curve are very close to each other in (b), while the low-v crossing is shifted to a position near the wave head in (a). In addition, we find that the v contours of wave-pinned pulses are qualitatively different for low and high v values. More specifically, low-v contours surround the pinned as well as the pinning pulse, while high-v contours define two, nonconnected areas.

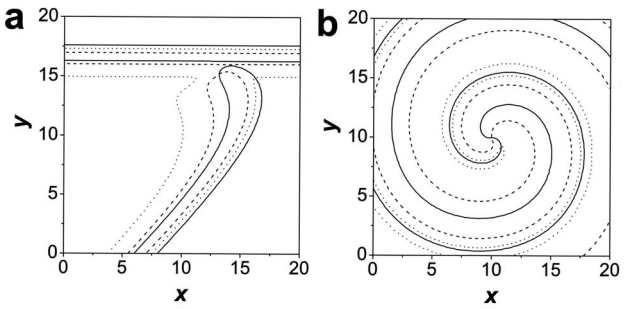

FIG. 5. Results of numerical simulations illustrating two qualitatively different, dynamic defects. The defect in (a) translates at steady speed in the wake of planar pulse. The defect in (b) rotates around a small circle and organizes a rotating spiral wave. The contour plots show curves of constants u and v where $u=0.1$ (solid), $v=0.1$ (dotted), and $v=0.3$ (dashed).

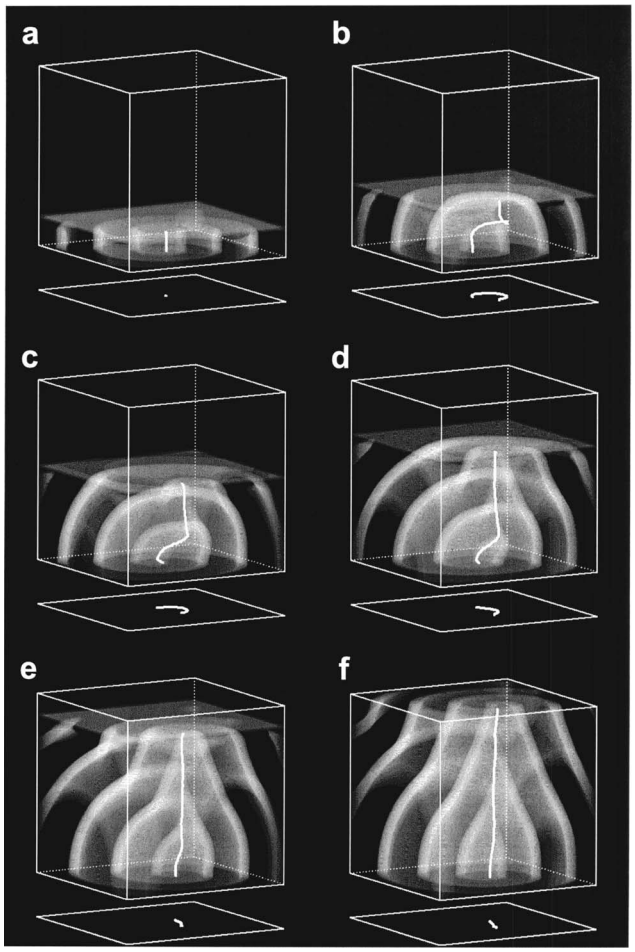

FIG. 6. Numerical simulation of a scroll wave filament pinned to a planar wave. The gray scale data show the spatial distribution of the variable u. The thick white curves are the filament. The squares underneath each box show the corresponding, two-dimensional projections of the filament. Time between subsequent frames: 7.5. Box size: $40\times40\times40$.

In the following, we explore whether Eqs. (1)–(3) can also reproduce the pinning of scroll wave filaments that we observe in our experiments with the CHD-BZ reaction (cf. Figs. 2 and 3). For this purpose, we carry out simulations in a spatially three-dimensional domain in which the initial conditions connect an untwisted scroll wave to a planar wave pulse. The first frame in Fig. 6 illustrates this unusual starting condition by visualizing the variable $u(x,y,z)$. For creating this pattern, we first compute the scroll wave solution as well as an upward moving, planar excitation pulse. These numerical solutions are then patched together with the scroll wave in the lowest portion $(0\leqslant z<5)$, followed by a volume slice $(5\leqslant z<7)$ containing the planar pulse solution and some of its tail. All points above the pulse front $(z\geqslant 7)$ are set to the steady state of the spatially homogeneous system.

The six frames in Fig. 6 show the evolution of the pattern initiated in the fashion described above. Superimposed onto the individual plots are white lines that represents the scroll wave filament. The projection of the latter space curves onto the system's lower boundary is shown below each box. The filament coordinates are identified as the points where the variables u and v are 0.5 and 0.2, respectively. The nonrotating, pinned wave ends in the back of the planar wave are not detected.

The data in Figs. 6(a) and 6(b) show that the initially straight filament quickly bends into a corkscrew-shaped curve. This early deformation is probably caused by the specific initial conditions of the simulation. More importantly, the subsequent frames in Fig. 6 clearly show that the filament remains pinned and expands upward at the speed of the planar wave. During this expansion process, the corkscrew-shaped deformation gradually disappears, thus, creating an essentially straight filament. Last, we observe that in Fig. 6(f) the planar wave has disappeared at the upper system boundary. This event connects the scroll wave and its filament to the upper boundary, creating a conventional scroll wave with a filament spanning the entire system in vertical direction.

The numerical result in Fig. 6 captures the main features of the experimental data in Fig. 2 as in both cases the scroll wave edge and its filament are pinned to a traveling wave. We also note that recently published experiments show that the total filament length of a pattern similar to Fig. 2 grows with twice the speed of its anchoring wave envelope.[30] This finding is in excellent agreement to our simulation where only one end of the filament is wave pinned and filament expansion occurs with half that speed.

To obtain information regarding the robustness of the overall pinning process, we varied the initial conditions in our simulations. Specifically, we increased the distance between the planar pulse and the scroll wave by filling in larger segments of the planar pulse tail. Qualitatively these trials revealed that the pinning process is sufficiently robust to be observable in experiments. However, pinning fails if the distance is too large, which manifests itself by rotation of the entire upper edge of the scroll wave. This rotational rather than translational motion creates a spiral-shaped, horizontal connection between the filament "stem" and the system's sidewalls. The overall shape of this unpinned filament and its dynamics are similar to the data in Figs. 8(c)–8(f).

Before we analyze the unwinding of the unpinned filament more closely, we first discuss the detailed wave structure of the pinned rotor. These details are difficult to discern from the images in Fig. 6, mainly because the system is several wavelengths wide. We, therefore, remove all outer waves by extracting the pattern within a narrow, cylindrical column surrounding the filament. Figure 7(b) shows the resulting view into the core of the pinned scroll wave. The disk-shaped object at the top belongs to the upward moving planar wave. Moreover, we find that the scroll wave is twisted, which implies that the phase ϕ of spiral rotation changes systematically as one moves along the filament in vertical direction z. The quantitative dependence $\phi(z)$ is shown in Fig. 7(a). The phase was determined by determining the angle ϕ for which the cross correlation between an arbitrary reference slice (here $z=5$) and the ϕ-rotated slice at height z is maximal. The data suggest a nearly linear dependence over the given filament length and possibly a slight decrease of the twist $d\phi/dz$ with increasing distance from the planar front.

The observation of pinned filaments raises several questions regarding the response of the filament to changes of the pinning wave pulse. The most drastic change is arguably the

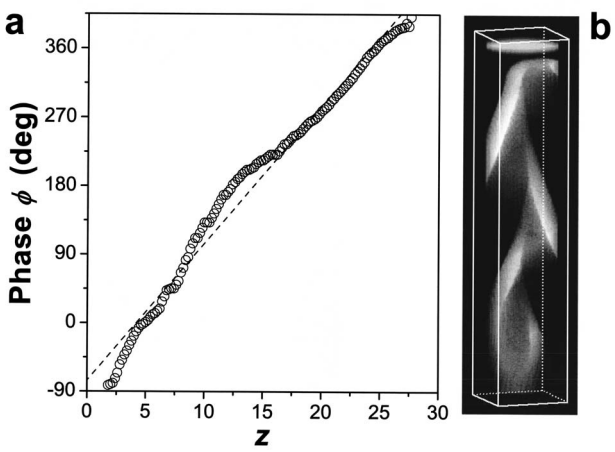

FIG. 7. Results of simulations showing that the pinned scroll wave is twisted. (a) Phase of spiral rotation as a function of distance z from the planar front. The dashed line compares the numerical results to their best-fit line. The positive slope indicates that the spiral $u_z(x,y)$ turns in forward direction as z increases. Rotation phases for $z>30$ correspond to the curved, lower part of the filament and are not analyzed. (b) Partial view of the data in Fig. 6(e) showing only the pattern within a cylindrical column (radius of 4.0) centered around the straight part of the filament.

annihilation of the wave. The image sequence in Fig. 8 shows an example for the latter scenario. The initial conditions and parameters in this simulations are identical to those in Fig. 6. However, a second planar wave is initiated at the upper boundary of the system [see Fig. 8(a)]. This wave propagates downward and collides with the upward moving scroll wave anchor. As expected for these excitation pulses, the collision causes the mutual annihilation of the planar waves and consequently the disappearance of the filament's anchor [Fig. 8(b)]. Furthermore, the upper edge of the scroll wave is now exposed to an initially refractory, wave-free space. As this space recovers its excitability, the wave edge moves upwards and begins to rotate. This rotation extends the straight rotation backbone of scroll wave along a spiral-shaped curve and connects it to the right, anterior boundary [Fig. 8(c)].

Shortly after the annihilation of the pinning wave pulse, the filament is highly curved, especially around the position of its earlier wave-terminated end. The subsequent filament dynamics decrease this curvature in a lassoing-type motion. More precisely, we find the central part of the spiral-shaped segment moves clearly downwards, while the end point at the right anterior surface shifts only slightly in upward direction. The downward motion in the central region creates a hooklike deformation [Fig. 8(e)]. The rotation of this deformation appears to be the main mechanism for unwinding the initially highly curved filament and can be seen clearly in the two-dimensional projections of the filament below the individual frames.

Last, we noticed an additional, but much shorter filament (not shown) in the upper left hand corner of the cubes in Figs. 8(c)–8(f). It can be discerned as a rotating wave edge. This filament extends from the left anterior to left posterior wall. It is not connected to the main rotation backbone because it resulted from an unconnected, curved segment of the scroll wave edge during the time of wave anchor annihilation. A similar but even shorter segment exists close to the upper, rear corner. It appears that these shorter filaments are pushed outward by the main vortex. This feature is reminiscent of a phenomenon in two-dimensional systems, where defects are known to drift in the wave field of larger spiral patterns.[42]

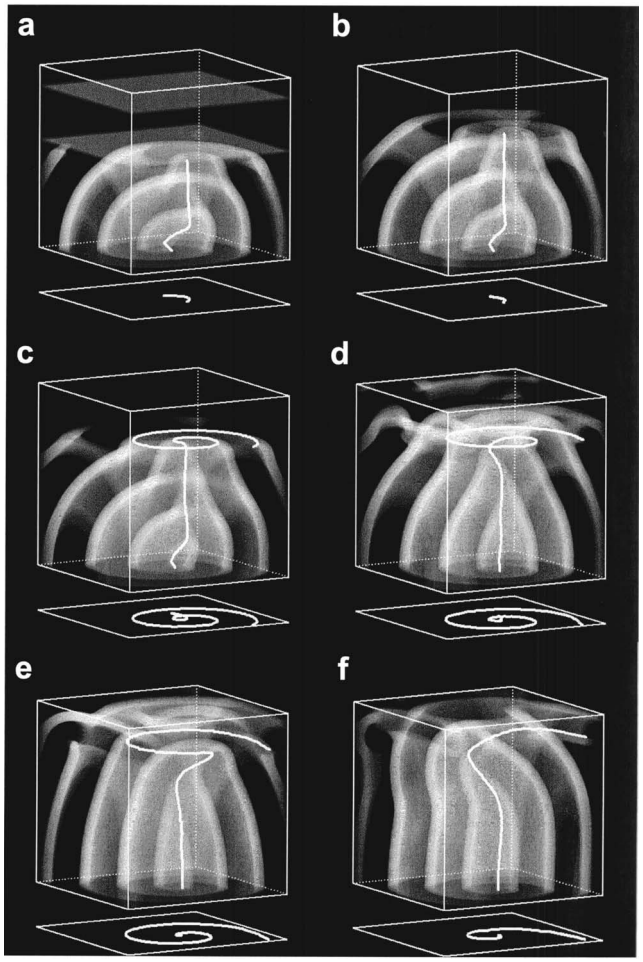

FIG. 8. Numerical simulation of a scroll wave filament pinned to a planar wave and of the dynamics induced by annihilation of that wave. The gray scale data show the spatial distribution of the variable u. The thick white curves are the filament. The squares underneath each box show the corresponding, two-dimensional projections of the filament. Time between frames (a) and (b) 6.25, (b) and (c) 1.25, (c) and (d) 13.75, (d) and (e) 27.5, and (e) and (f) 117.5. Box size: $40\times40\times40$.

VI. CONCLUSIONS

Our results show that a certain type of anomalous dispersion, known as "wave merging," can allow the pinning of scroll wave filaments to traveling wave pulses. This finding extends earlier views that required filaments to end in the system boundary or trace topologically closed space curves such as circles and knots.[27,28] The fact that wave-pinned filaments are readily observed in experiments and numerical simulations suggests that the phenomenon is sufficiently stable and its initial conditions easily accessible.

We also showed that filament pinning is closely tied to the existence of nonrotating, translational defects. These defects are observed in two-dimensional as well as three-dimensional media (cf., Figs 1–3). In both cases, they be-

come nontranslating, rotating spirals upon removal of their anchor wave, which we realized by collision with other wave pulses. However, the resulting dynamics in three-dimensional systems is clearly richer than in their two-dimensional counterparts.

The numerical simulations presented here show only a simple example for the dynamics one can expect to arise from the annihilation of the anchoring wave pulse. Another interesting but nonetheless simple scenario is the case of a scroll wave confined and pinned to an expanding spherical wave. It is not apparent how the termini of the filament move under such conditions. It is also not clear how such a structure responds to the annihilation of the pinning wave, but we believe that an unknotted filament loop will be created.

Last, we note that phenomena similar to wave-pinned filaments could also exist in systems with finite bandwidth dispersion relations. This anomaly has been observed in experiments and simulations and leads to unusual wave behavior known as "wave tracking."[37,43] The latter term refers to the dynamics of wave trains that expand despite the periodic annihilation of their outermost wave pulse. We suggest that for these conditions, scroll wave filaments might possibly end at the periphery of their wave-filled domains. However, clearly more studies are needed to develop a good understanding of nonconventional filament end points, their dynamics and stability.

ACKNOWLEDGMENTS

This work has been supported by the National Science Foundation under Grant No. 0513912.

[1] M. Assenheimer and V. Steinberg, Nature (London) **367**, 345 (1994).
[2] L. F. Dong, F. C. Liu, S. H. Liu, Y. F. He, and W. L. Fan, Phys. Rev. E **72**, 046215 (2005).
[3] K. Agladze and O. Steinbock, J. Phys. Chem. A **104**, 9816 (2000).
[4] C. Punckt, F. S. Merkt, and H. H. Rotermund, New J. Phys. **9**, 213 (2007).
[5] *Chemical Waves and Patterns*, edited by R. Kapral and K. Showalter (Kluwer, Dordrecht, 1995).
[6] S. C. Müller, T. Mair, and O. Steinbock, Biophys. Chem. **72**, 37 (1998).
[7] J. D. Lechleiter, L. M. John, and P. Camacho, Biophys. Chem. **72**, 123 (1998).
[8] M. A. Dahlem and S. C. Müller, Ann. Phys. **13**, 442 (2004).
[9] *Focus Issue: Cardiovascular Physics*, Chaos **17**(1) (2007).
[10] A. Hagberg and E. Meron, Nonlinearity **7**, 805 (1994).
[11] Exceptions have been reported. See, e.g., L. F. Yang and I. R. Epstein, J. Phys. Chem. A **106**, 11676 (2002).
[12] O. Steinbock and S. C. Müller, Physica A **188**, 61 (1992).
[13] J.-M. Flesselles, A. Belmonte, and V. Gáspár, J. Chem. Soc., Faraday Trans. **94**, 851 (1998).
[14] J. Rinzel and K. Maginu, in *Nonequilibrium Dynamics in Chemical Systems*, edited by C. Vidal and A. Pacault (Springer, Berlin, 1984), pp. 107–113.
[15] M. Falcke, M. Or-Guil, and M. Bär, Phys. Rev. Lett. **84**, 4753 (2000).
[16] G. Bordiougov and H. Engel, Phys. Rev. Lett. **90**, 148302 (2003).
[17] G. Roder, G. Bordyugov, H. Engel, and M. Falcke, Phys. Rev. E **75**, 036202 (2007).
[18] J. Christoph, M. Eiswirth, N. Hartmann, R. Imbihl, I. Kevrekidis, and M. Bär, Phys. Rev. Lett. **82**, 1586 (1999).
[19] N. Manz, S. C. Müller, and O. Steinbock, J. Phys. Chem. A **104**, 5895 (2000).
[20] C. T. Hamik, N. Manz, and O. Steinbock, J. Phys. Chem. A **105**, 6144 (2001).
[21] C. T. Hamik and O. Steinbock, New J. Phys. **5**, 58 (2003).
[22] J. P. Keener, Physica D **31**, 269 (1988).
[23] B. Echebarria, V. Hakim, and H. Henry, Phys. Rev. Lett. **96**, 098301 (2006).
[24] M. Vinson, S. Mironov, S. Mulvey, and A. Pertsov, Nature (London) **386**, 477 (1997).
[25] S. Alonso, F. Sagués, and A. S. Mikhailov, J. Phys. Chem. A **110**, 12063 (2006).
[26] T. Bánsági, Jr. and O. Steinbock, Phys. Rev. E **76**, 045202 (2007).
[27] A. M. Pertsov, M. Wellner, M. Vinson, and J. Jalife, Phys. Rev. Lett. **84**, 2738 (2000).
[28] H. Zhang, B. Hu, B.-W. Li, and Y.-S. Duan, Chin. Phys. Lett. **24**, 1618 (2007).
[29] P. M. Sutcliffe and A. T. Winfree, Phys. Rev. E **68**, 016218 (2003).
[30] T. Bánsági, Jr., C. Palczewski, and O. Steinbock, J. Phys. Chem. A **111**, 2492 (2007).
[31] B. T. Ginn, B. Steinbock, M. Kahveci, and O. Steinbock, J. Phys. Chem. A **108**, 1325 (2004).
[32] A. T. Winfree, S. Caudle, G. Chen, P. McGuire, and Z. Szilagyi, Chaos **6**, 617 (1996).
[33] U. Storb, C. R. Neto, M. Bär, and S. C. Müller, Phys. Chem. Chem. Phys. **5**, 2344 (2003).
[34] T. Bánsági, Jr. and O. Steinbock, Phys. Rev. Lett. **97**, 198301 (2006).
[35] A. S. Mikhailov, *Foundations of Synergetics I* (Springer, New York, 2002).
[36] O. Steinbock, V. S. Zykov, and S. C. Müller, Phys. Rev. E **48**, 3295 (1993).
[37] N. Manz, C. T. Hamik, and O. Steinbock, Phys. Rev. Lett. **92**, 248301 (2004).
[38] N. Manz, B. T. Ginn, and O. Steinbock, Phys. Rev. E **73**, 066218 (2006).
[39] D. Barkley, Physica D **49**, 61 (1991).
[40] H. J. Krug, L. Pohlmann, and L. Kuhnert, J. Phys. Chem. **94**, 4862 (1990).
[41] R. J. Field and R. M. Noyes, J. Chem. Phys. **60**, 1877 (1974).
[42] I. Schebesch and H. Engel, Phys. Rev. E **60**, 6429 (1999).
[43] N. Manz and O. Steinhbock, J. Phys. Chem. A **108**, 5295 (2004).